

University of Groningen

## Lead Sulfide Quantum Dots for Synaptic Transistors

Tran, Karolina; Wang, Han; Pieters, Meike; Loi, Maria Antonietta

*Published in:*  
Advanced Intelligent Systems

*DOI:*  
[10.1002/aisy.202300218](https://doi.org/10.1002/aisy.202300218)

**IMPORTANT NOTE: You are advised to consult the publisher's version (publisher's PDF) if you wish to cite from it. Please check the document version below.**

*Document Version*  
Publisher's PDF, also known as Version of record

*Publication date:*  
2023

[Link to publication in University of Groningen/UMCG research database](#)

*Citation for published version (APA):*

Tran, K., Wang, H., Pieters, M., & Loi, M. A. (2023). Lead Sulfide Quantum Dots for Synaptic Transistors: Modulating the Learning Timescale with Ligands. *Advanced Intelligent Systems*, 5(11), Article 2300218. <https://doi.org/10.1002/aisy.202300218>

**Copyright**

Other than for strictly personal use, it is not permitted to download or to forward/distribute the text or part of it without the consent of the author(s) and/or copyright holder(s), unless the work is under an open content license (like Creative Commons).

The publication may also be distributed here under the terms of Article 25fa of the Dutch Copyright Act, indicated by the "Taverne" license. More information can be found on the University of Groningen website: <https://www.rug.nl/library/open-access/self-archiving-pure/taverne-amendment>.

**Take-down policy**

If you believe that this document breaches copyright please contact us providing details, and we will remove access to the work immediately and investigate your claim.

*Downloaded from the University of Groningen/UMCG research database (Pure): <http://www.rug.nl/research/portal>. For technical reasons the number of authors shown on this cover page is limited to 10 maximum.*

# Lead Sulfide Quantum Dots for Synaptic Transistors: Modulating the Learning Timescale with Ligands

Karolina Tran, Han Wang, Meike Pieters, and Maria Antonietta Loi\*

One of the emerging paradigms to resolve pressing issues of modern computing electronics, such as limits in miniaturization and excessive energy consumption, takes inspiration from the biological brain and is therefore expected to display some of its properties, such as energy efficiency and effective learning. Moreover, one of the brain's remarkable properties is its ability to process complex information by resolving it on different timescales. In synapse-emulating artificial devices, some form of memory (e.g., hysteresis in current–voltage characteristics) is required. One of the important characteristics of biological synapses is the coexistence of short- and long-term memory, also called plasticity. However, a broader exploration of memory at multiple timescales in materials remains limited. Herein, the first example of synaptic transistors utilizing colloidal quantum dots (CQDs) as active material is reported. It is demonstrated that PbS-CQDs, with metal halide and perovskite-like ligands, are ideal as an active material for synaptic transistors exhibiting both short- and long-term plasticity. Most interestingly, by changing the chemistry of the quantum dot outer monolayer, a drastic change in the temporal response of the learning is observed, demonstrating the possibility of engineering materials exhibiting learning at multiple timescales, similar to the biological synapses.

consumption in ICT is big data and artificial intelligence algorithms. The existing CMOS-based hardware is versatile and able to perform a multitude of tasks, however, due to its inherent nature of having memory and processing units separated, it is power-hungry when it comes to tasks like machine learning. In the search for new computing paradigms that could overcome these limitations, the biological brain has emerged as one of the main inspirations. Therefore, materials and device architectures that can emulate the behavior of neurons and synapses are the target of this emerging research field. An example of a device emulating synapses is the memristor—a resistor with a memory, described by Chua as a two-terminal device with a pinched hysteresis loop in its current–voltage characteristics.<sup>[4]</sup> However, three-terminal devices (transistor-like) have also been demonstrated to show interesting properties to emulate synapses. The basic condition is always that they exhibit hysteretic behavior. However,

the availability of three terminals can allow better control of the functionality as the addition of the third terminal may influence the number of available conduction states by modulating its bias. Moreover, the interaction of the active material with the dielectric material itself can induce other features, such as charge-trapping on the dielectric-semiconductor interface, ion doping, ion-gating, etc.

While, two-terminal devices remain the most popular implementation for history-dependent synaptic devices,<sup>[5]</sup> a great effort in the transistor implementations, such as floating-gate transistors,<sup>[6–8]</sup> photo-gated and photo-responsive structures,<sup>[9–11]</sup> and charge-trapping based field-effect transistors (FETs)<sup>[12,13]</sup> resulted in synaptic transistors breaking through to the mainstream.

Considering implementation, one of the major advantages of transistor geometry over the memristor one is that the transistor architecture removes the necessity of a driving circuit crucial for memristors. A further important advantage of the transistor geometry is the increased control of the device response that can be achieved by the introduction of the third terminal, including the possibility of correcting for degradation of the device characteristics.


One of the critical features of the brain is activity on different timescales.<sup>[14–17]</sup> These timescales are associated with different types of neural processing and computation, such as sensation, perception, action, learning, and memory. Depending on the

## 1. Introduction

The estimated global energy consumption share of the information and communication technology sector (ICT) was 3.6% in 2015,<sup>[1]</sup> and despite the discrepancies in their estimates among experts, different sources agree this fraction will increase in the future.<sup>[1–3]</sup> One of the growing concerns regarding energy

K. Tran, H. Wang, M. Pieters, M. A. Loi  
Photophysics and OptoElectronics  
Zernike Institute for Advanced Materials  
University of Groningen  
Nijenborgh 4, 9747 AG Groningen, The Netherlands  
E-mail: m.a.loi@rug.nl

K. Tran, M. A. Loi  
Groningen Cognitive Systems and Materials Centre (CogniGron)  
University of Groningen  
9747 AG Groningen, The Netherlands

 The ORCID identification number(s) for the author(s) of this article can be found under <https://doi.org/10.1002/aisy.202300218>.

© 2023 The Authors. Advanced Intelligent Systems published by Wiley-VCH GmbH. This is an open access article under the terms of the Creative Commons Attribution License, which permits use, distribution and reproduction in any medium, provided the original work is properly cited.

DOI: 10.1002/aisy.202300218

brain region and neuron type, the brain shows a complex temporal hierarchy of information processing. The concept of intrinsic neural timescales (INT) has been suggested to play an important role in input encoding,<sup>[15]</sup> making it another point of consideration in the physical implementation of large-scale neuromorphic platforms. Recent literature contains many examples of two- and three-terminal devices exhibiting long- and short-term memory.<sup>[12,18–21]</sup> However, to the authors' best knowledge, multitime-scale behavior has only been demonstrated on a single platform, without interfering with the nature of the active material or the physical dimensions of the device (vide infra) in a ferroelectric hafnium-zirconium oxide (HZO),<sup>[22]</sup> and is yet to be addressed in devices with solution-processable active layers which are known for their processability simplicity.

The unique optoelectronic properties of colloidal quantum dots (CQDs) made of this class of materials a topic of intense application-driven research. CQDs are successfully applied at the industrial level on displays and photodetectors, and at the research level have been investigated in solar cells,<sup>[23–28]</sup> light-emitting diodes, field-effect transistors,<sup>[24,29–33]</sup> and very widely in photodetectors.<sup>[8,34–37]</sup> One notable advantage of CQDs is their design flexibility, not limited to chemical composition<sup>[38–41]</sup> but, more importantly, to size<sup>[42,43]</sup> and surface chemistry.<sup>[44–47]</sup> One of the workhorses of the field is lead-sulfide-based nanocrystals, PbS CQDs, because of their highly reproducible chemistry and their broad tunability (from the visible to the short wavelength infrared) of the absorption.<sup>[48–50]</sup>

Colloidal quantum dots have been applied in various neuromorphic devices: in transistor architecture<sup>[8,51,52]</sup> as an additional charge-trapping layer within the dielectric and in two-terminal devices.<sup>[53–55]</sup> However, field-effect transistors with a sole quantum dot active layer without the exploitation of their optical

activity seem to have been rarely explored in this field,<sup>[56]</sup> even though they often exhibit large current hysteresis.<sup>[24,31,32]</sup> In this work, we utilize bottom-gate-bottom-contact FET structure with blade-coated film of PbS CQDs, and demonstrate that colloidal quantum dots are not only suitable active material for synaptic transistors by exhibiting short-term (excitatory postsynaptic current tracking (EPSC), paired-pulse facilitation (PPF)) and long-term (spike-timing-dependent plasticity (STDP)) plasticity but also exhibit different neuromorphic behavior when different ligands are utilized on their surface, fitting the concept of internal neural timescales on the same material platform. Furthermore, the advantage of our approach lies in the structural simplicity of the device and the solution-processability of the active material which may make this approach preferred over more complex one.

## 2. Results and Discussion

Memristors and synaptic transistors have been proposed as devices to emulate the functionalities of synapses. To fully explore the advantage of the third terminal, in analogy to a biological synapse (Figure 1A), we devise the gate electrode to provide presynaptic signals (presynapse), while the source–drain electrodes will give a postsynaptic channel (postsynapse). In such a scheme, the presynapse gradually modulates the response of the postsynapse. In biology, synapses connect neurons, determining the information transfer in our nervous system. Their strength (called weight) results from the information transfer history from a presynaptic to a postsynaptic side. The changes in synaptic strength, or synaptic plasticity, are crucial to the learning and problem-solving processes occurring in the brain. Generally, two types of synaptic plasticity are distinguished, the so-called long term and short term. The latter refers mainly to working memory processes,

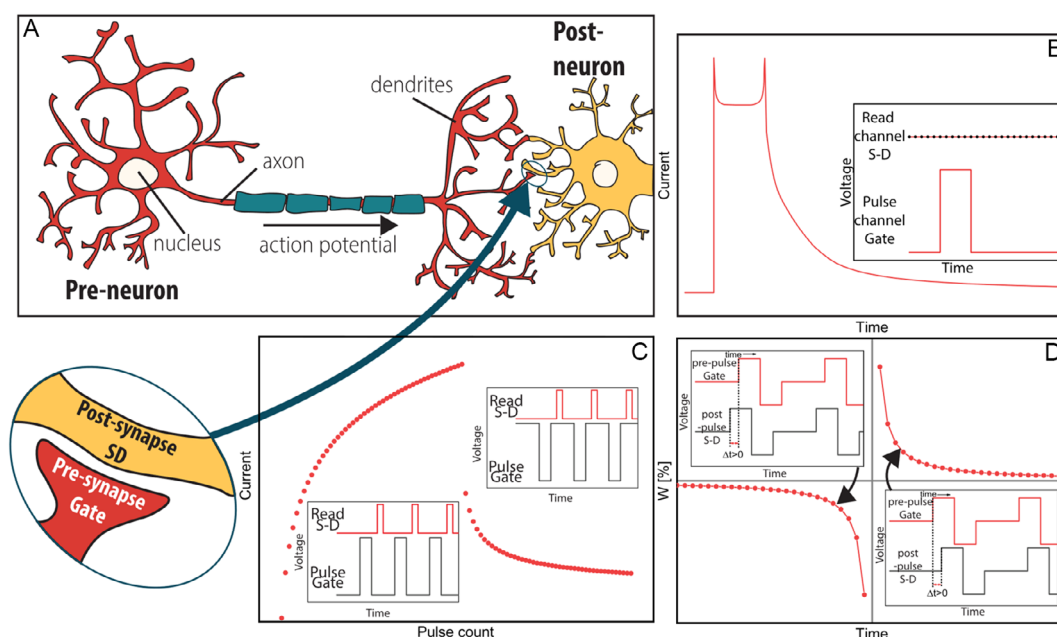


**Figure 1.** A) A simplified neuron model with a close-up of a synapse and corresponding terminals of a field-effect transistor. B–D) Schematic representation of three learning protocols with ideal sample response and input wavefunctions (insets): (B) Excitatory postsynaptic current tracking (EPSC), (C) paired-pulse facilitation (PPF), and (D) spike-timing-dependent plasticity (STDP).

while the former to long-lasting memory storage.<sup>[57,58]</sup> These features can be studied by a variety of learning protocols, such as PPF and EPSC for short-term effects, and STDP and spike-rate-dependent plasticity (SRDP) for long-term plasticity. Schematics of selected learning protocols applied to the CQD-FET devices in this work are shown in Figure 1B–D. The graphs show simulated responses of each test, while the insets represent biasing scheme for each terminal. In all cases, we apply rectangular voltage stimuli to the gate (presynaptic) channel. In EPSC and PPF tracking, the pulses are unipolar with respect to the baseline voltage (where  $V_{G \text{ base}} = 0 \text{ V}$ , unless indicated otherwise). In contrast, in STDP, to ensure the decoupling of consecutive pulses, the fillip consisted of positive and negative parts, as presented in the inset of Figure 1D.

Our synaptic transistor was fabricated using a bottom-gate bottom-contact configuration and the active material consisting of ink of CQDs was deposited by blade coating. As CQDs have seldomly reported for this application, in the following, we briefly describe the nature of the sample and the general device characteristics.

The starting CQD sample is stabilized by oleic acid molecules. Due to their size, they hinder electronic transport between quantum dots. Thus, the first step to facilitate charge transport among the single QDs is to decrease the dot-to-dot distance by exchanging oleic acid (OA) for smaller moieties. Here, we utilized the

so-called solution-phase ligand exchange (see ref. [22] for more details on the procedure) (Figure 2A) with two types of ligands, a mixture of lead halides and ammonium acetate, denoted as PbS-PbX<sub>2</sub>/AA, and methylammonium lead triiodide (PbS-MAPbI<sub>3</sub>).<sup>[23,59]</sup> In PbS-PbX<sub>2</sub>/AA QDs, halide anions (I<sup>-</sup> and Br<sup>-</sup>) coordinate quantum dot facets, while in PbS-MAPbI<sub>3</sub> iodoplumbate (PbI<sub>3</sub><sup>-</sup>) anions are responsible for this function. Ammonium-containing species (NH<sub>3</sub><sup>+</sup> and CH<sub>3</sub>NH<sub>3</sub><sup>+</sup> (referred to as MA<sup>+</sup>)) maintain charge neutrality and colloidal stability of the inks forming a sort of double layer. Excess ligands should be removed for optimal device performance, as they can participate in charge-trapping, effectively hindering charge transport, and possibly modifying the temporal dynamics of the devices.<sup>[59,60]</sup> We verify whether the ligand exchange was performed successfully without disrupting the quantum confinement through absorption spectroscopy (Figure 2B). The redshift of the LE samples with respect to PbS-OA CQDs can be attributed to a different dielectric constant of the environment, as the two inks in DFP have their maximum at the same wavelength (DFP has dielectric constant  $\epsilon$  of 107.8; while hexane has 1.886<sup>[61]</sup>). The apparent broadening of the PbS-MAPbI<sub>3</sub> CQDs suggests increased attachment of the quantum dots within the ink compared to the PbS-PbX<sub>2</sub>/AA variation.<sup>[31]</sup>

The transistor characteristics of the two inks show some dissimilarities (see Figure 2C) due to the different passivation

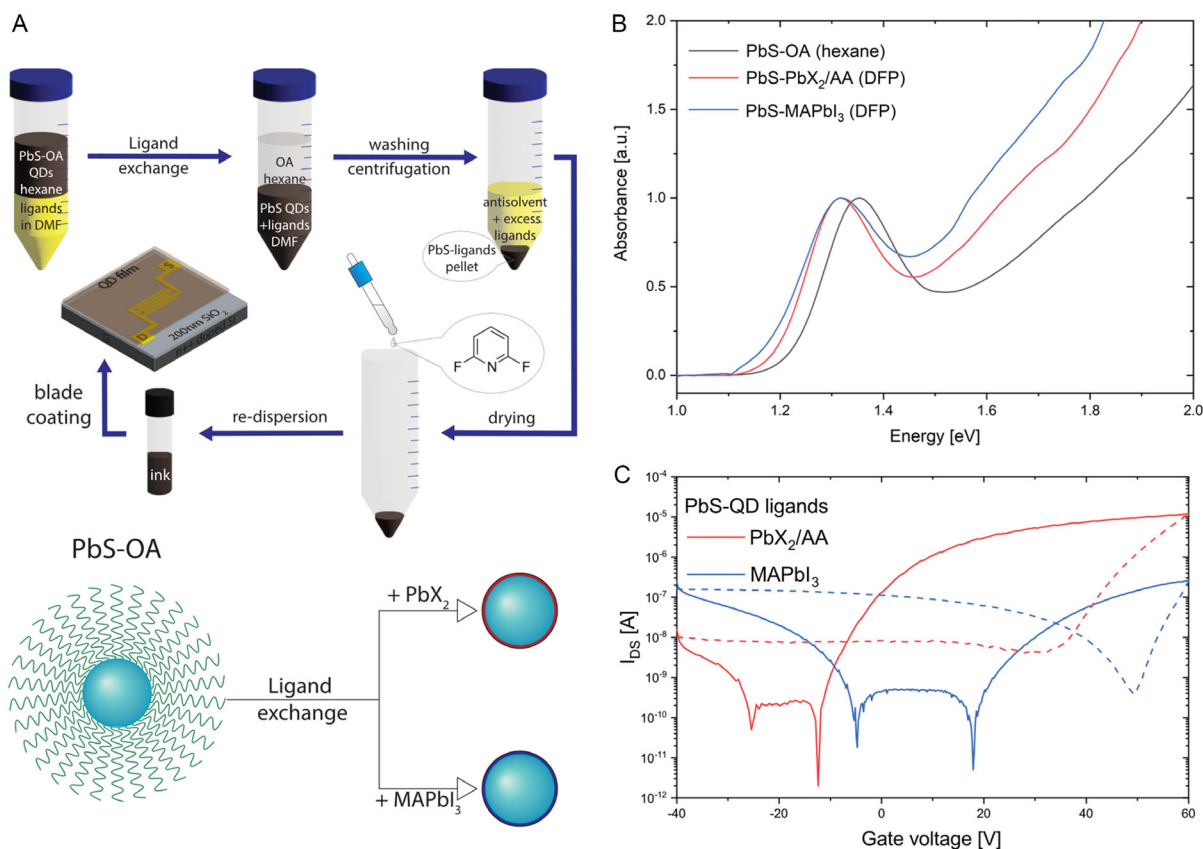


**Figure 2.** A) Schematic representation of the ligand exchange process leading to the two CQD inks. B) Normalized absorption spectra of the native solution (PbS-OA) in hexane and of the two inks after ligand exchange with corresponding new ligands (PbX<sub>2</sub> and MAPbI<sub>3</sub>) in difluoropyridine (DFP). C) Transfer characteristics of devices made with PbS-PbX<sub>2</sub>/AA and PbS-MAPbI<sub>3</sub>.

provided by the ligands on their surface and of the above-mentioned QD attachment of one of the solutions.

Factors such as surface traps on the QD surface, O–H groups in the SiO<sub>2</sub> surface, incomplete removal of excess ligands, and an inhomogeneous energy landscape of quantum dots, are factors that give rise to hysteresis in the transistor transfer characteristics in Figure 2C, which can be considered a device's inherent memory. To investigate which of the two type of QD-FETs is the fittest as synapses, we performed three learning tests: excitatory postsynaptic current tracking (EPSC, **Figure 3**), paired-pulse facilitation (PPF, **Figure 4**), with the two being a manifestation of short-term plasticity,<sup>[62]</sup> and spike-time-dependent plasticity (STDP, **Figure 5**) being a manifestation of long-term plasticity.<sup>[63]</sup>

Starting with EPSC, we apply a voltage pulse of  $-20$  V, 5–100 ms long, to the gate and probe the source–drain channel response before, during, and after the pulse to observe the state retention of every single pulse. The baseline gate voltage was set to 0 V. In these measurements, we observe that both devices, the one based on PbS–PbX<sub>2</sub>/AA (Figure 3A) and the one based on PbS–MAPbI<sub>3</sub> (Figure 3B), show certain state retention for the short, 5 ms pulses. The current remains one order of magnitude higher than the initial value (first pulse was applied at 0.05 s into the measurement) 20–30 ms after stimuli removal, but the different discharge behavior (with the increase of the signal for the PbS–PbX<sub>2</sub> sample after about 5 ms from the initial decay) after stimulus removal is an effect of the choice of the read voltage. While in both cases, the pulsing occurs in the positive hysteresis loop (an increase of channel conductance in reverse sweep compared to forward sweep) of their transfer characteristics (Figure S1C, Supporting Information), the readout takes place at 0 V V<sub>G</sub>, which for PbS–PbX<sub>2</sub>/AA sample means a shift to the negative loop. Hence, the initial dip in the current value shows a minimal influence of the read voltage. When the pulse duration was increased to 100 ms (Figure 3C), the PbS–MAPbI<sub>3</sub> QD FET current decayed to the initial state almost instantaneously, while the PbS–PbX<sub>2</sub>/AA sample's current decreased rapidly right after the stimulus removal only to rebound to  $\approx 230\%$  initial current and decline exponentially to reach the base value after approximately 800 ms, emphasizing, even more, the temporal behavior differences between the two sets of samples.

If we increase the number of applied pulses, we can observe whether the close proximity of same-polarity pulses triggers short-term plasticity behavior. In this experiment (PPF, Figure 4A,B), we used 500 or 1,000 pulse trains of 30 or 25 V to the gate of PbS–MAPbI<sub>3</sub> and PbS–PbX<sub>2</sub>/AA, respectively, followed by the same number of pulses of the opposite polarity ( $-30$  or  $-25$  V). We repeated this experiment several times with a different pulse duration spanning from 10 to 500 ms. Both measured devices show potentiation of the signal with the negative pulse ( $-30$  or  $-25$  V) and depression with positive pulses. In both cases, the reset to the initial state is very fast, and there is no clear indication of a gradual decrease from the low-resistance state, emphasizing response asymmetry in single devices. The potentiation part of the PbS–MAPbI<sub>3</sub> device shows an increase in the source–drain current, however, as the number of pulses grows, the signal decreases. This trend is similar for 10 and 100 ms pulses with a slight difference in the current magnitude. In contrast, the PbS–PbX<sub>2</sub>/AA device reveals a strikingly

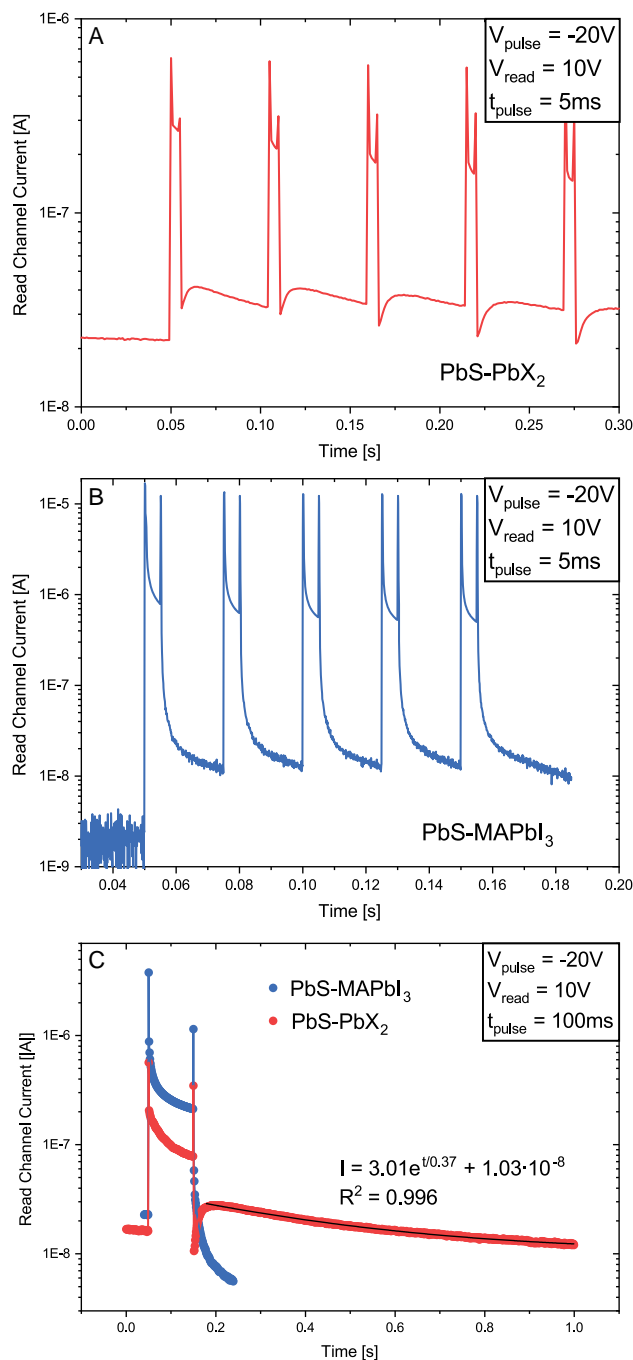


**Figure 3.** EPSC tracking. 5 ms pulses applied to A) PbS–PbX<sub>2</sub> FET and B) PbS–MAPbI<sub>3</sub> devices. C) 100 ms pulse tracking. All devices were subjected to  $-20$  V gate bias and  $+10$  V source–drain (read) voltage.

different behavior. While similar to the PbS–MAPbI<sub>3</sub>, it potentiates with a negative gate bias, in contrast, we observe a clear build-up of current with increasing pulse length. The attenuation is very small when a short pulse is utilized, however, it increases linearly with pulse time (Figure S1, Supporting Information). For this material, we establish the PPF index (Table S1, Figure S2, Supporting Information) as  $\left(1 + \frac{I_{SD,initial} - I_{SD,max}}{I_{SD,initial}}\right) \times 100\%$ , where

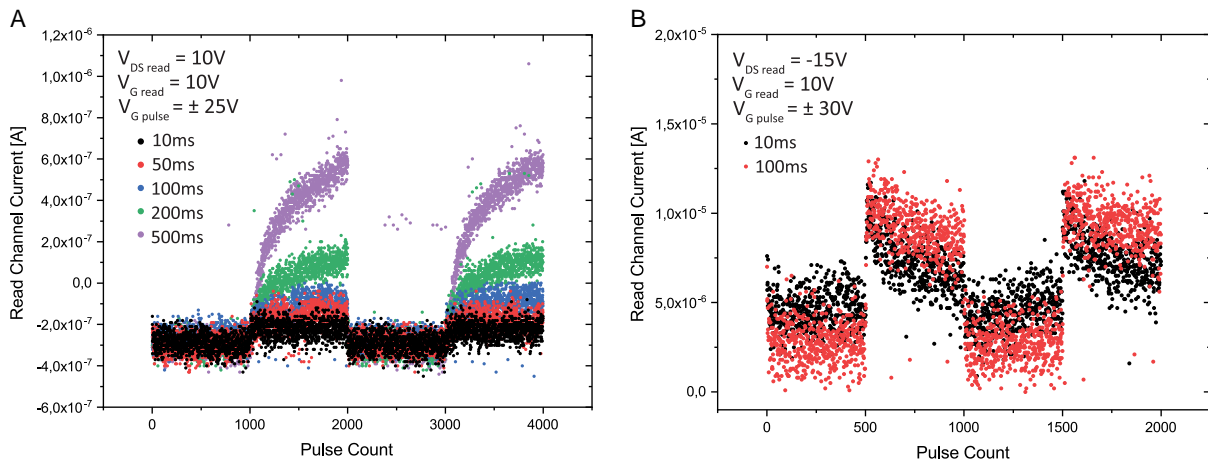


**Figure 4.** Paired-pulse facilitation experiment—two-cycle PPF data for A) PbS–PbX<sub>2</sub>/AA and B) PbS–MAPbI<sub>3</sub> for different pulse lengths. Both materials show potentiation when subjected to negative pulses while being reset with positive pulses.

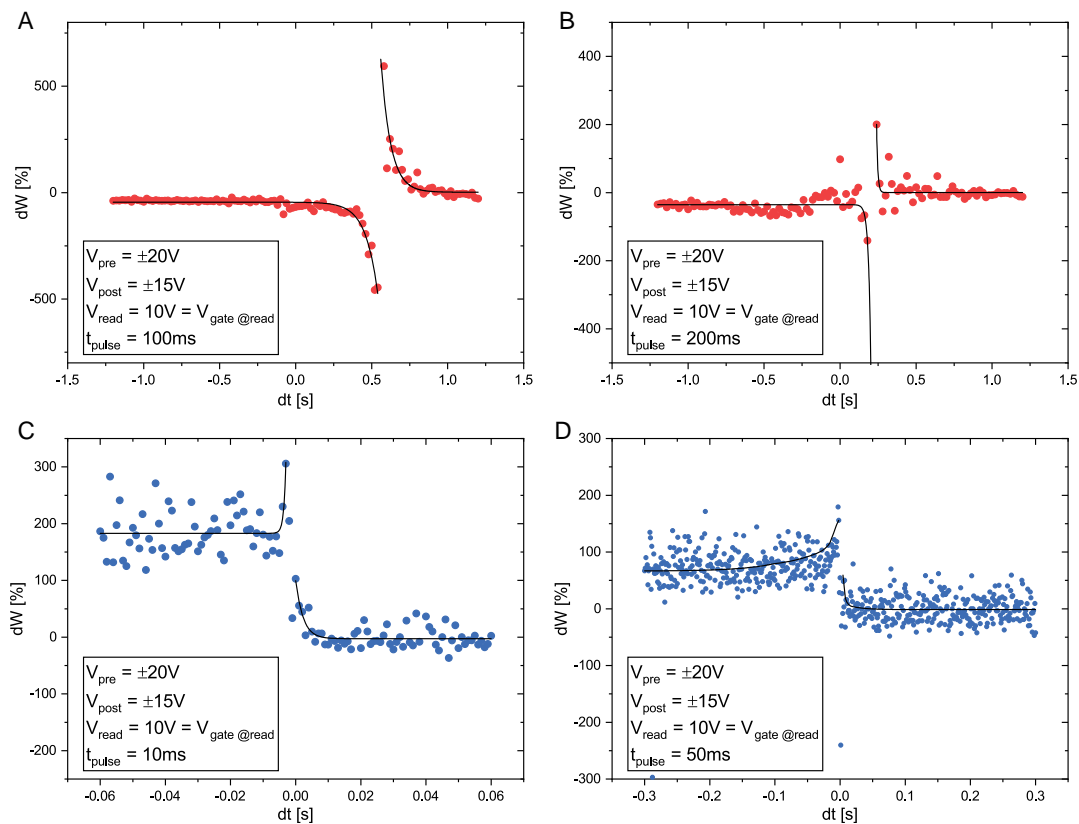


**Figure 5.** STDP measurements of the FET devices. A,B) for PbS–PbX<sub>2</sub>/AA QDs; C,D) for PbS–MAPbI<sub>3</sub> QDs. The legends include a biasing scheme of the devices and pulse duration.

$I_{SD,initial}$  is the current at the start of the pulse train sequence, and  $I_{SD,max}$  is the current at the last point of the potentiation sequence, as a maximum potentiation is reached at the end of the potentiation curve. For short pulses of 10 ms, the PPF index was only 4% higher than the initial value. However, for longer pulses, the potentiation was significantly larger, achieving values as large as 263% for 200 ms pulses and 436% for 500 ms ones.

To study long-term memory in PbS QD-based devices, STDP measurements were performed (Figure 5). In this experiment, we tracked the change in synaptic weight expressed as  $dW = \frac{I_{SD,after} - I_{SD,before}}{I_{SD,before}} \times 100\%$ , as the overlap between two incoming pulses, one from the presynaptic channel (gate) and the postsynaptic channel (source–drain), varies as a function of the temporal distance between the two. Scanning was performed

starting with large positive difference between pre- and postsynaptic pulses (from right to left on the graphs). Both types of devices exhibit learning – PbS–PbX<sub>2</sub>/AA (Figure 5A,B), PbS–MAPbI<sub>3</sub> (Figure 5C,D). The PbS–PbX<sub>2</sub>/AA device shows long-term potentiation (LTP) when the presynaptic pulse comes ahead of the postsynapse ( $\Delta t > 0$ ) and long-term depression (LTD) when the latter precedes it ( $\Delta t < 0$ ). For the PbS–MAPbI<sub>3</sub> device, the trend is the opposite, however, a steep change around  $\Delta t = 0$  suggests long-term behavior to be less likely. Moreover, scanning from  $\Delta t > 0$  to  $\Delta t < 0$ , we observe a change in the baseline after reaching the turning point at  $t = 0$ . The mirroring of the asymmetry most likely comes from the positioning in hysteresis loops with respect to the read voltage ( $V_{\text{read}}$ ). 10 V read voltage falls in the clockwise hysteresis loop of PbS–PbX<sub>2</sub>/AA FET, while the same bias in the PbS–MAPbI<sub>3</sub> is within the counterclockwise hysteresis loop. Moreover, the STDP was found to occur only in certain time ranges for the two materials. For PbS–MAPbI<sub>3</sub> QD FETs, only relatively short pulses, 10–50 ms, resulted in STDP, while the opposite was true for PbS–PbX<sub>2</sub>/AA QD FETs, which showed desired behavior at longer, 100–200 ms pulses. It is also worth mentioning that the asymmetry of the PbS–PbX<sub>2</sub>/AA STDP plot also appears in the temporal axis. The inversion points of this device are always shifted away from zero. The cause of this phenomenon remains unclear, whether this is an inherent property of the material or device, or a measurement issue.

### 3. Conclusion

In this work, we demonstrated two types of field-effect transistors with lead sulfide quantum dots as an active material. The change of the ligands on the QDs drastically changes the electrical properties of the devices, such as charge carrier mobility and threshold voltage. Importantly, these devices demonstrate synaptic behavior, such as paired-pulse facilitation (short-term plasticity) and STDP (long-term plasticity) as a result of charge-trapping on the QD surface and the QD–dielectric interface.

We found the two systems' active layers to act on different timescales, the PbS–MAPbI<sub>3</sub> QD FET showed synaptic plasticity upon short, 10 ms range pulses, while the PbS–PbX<sub>2</sub>/AA QD FET is strongly stimulated with long pulses from 100 up to 500 ms width, making QD FETs a unique platform to emulate internal neural timescales found in a biological brain.

### 4. Experimental Section

**QD Synthesis:** A hexane dispersion of PbS CQDs with oleic acid ligands (PbS-OA CQDs) was used as a starting material for ink preparation. The synthesis and purification of the PbS-OA CQDs were done in accordance with other works.<sup>[64,65]</sup>

**PbS–PbX<sub>2</sub>/AA QD Ink:** In the case of PbS–PbX<sub>2</sub>/AA ink, the ligand components, PbI<sub>2</sub> (lead iodide 99.99%, TCI), PbBr<sub>2</sub> (TCI), and COOCH<sub>3</sub>NH<sub>4</sub> (AA, ammonium acetate, Sigma-Aldrich), were first dissolved in DMF to 0.1, 0.04, and 0.06 M respectively, and then combined in a vial with 10 mg mL<sup>-1</sup> PbS-OA CQDs suspension in hexanes. The vial with the two immiscible liquids was shaken vigorously until the top layer (hexanes) was transparent. The following step included the removal of the hexanes with oleic acid and washing the mixture with additional hexanes. As produced, CQD/DMF suspension was then centrifuged with the addition of toluene as an antisolvent (1:2 volume ratio with respect to the initial

volume of DMF) to remove excess ligand precursors, dried and redispersed in DFP (difluoropyridine) to obtain 50 mg mL<sup>-1</sup> concentration.

**PbS–MAPbI<sub>3</sub> QD Ink:** For PbS–MAPbI<sub>3</sub> ink, methylammonium hydroiodide (MAI, CH<sub>3</sub>NH<sub>2</sub>·HI, TCI) and PbI<sub>2</sub> were used as ligand precursors. In the first step, similarly, as for the PbS–PbX<sub>2</sub>/AA QD ink, the ligand components were dissolved in DMF, both to 0.05 M. After combining with the 10 mg mL<sup>-1</sup> PbS-OA QD in hexanes, the mixture was left to stir at room temperature and 500 RPM overnight. The next day the hexane fraction was removed and the remaining part was washed and centrifuged with the antisolvent (acetone) as described for the PbS–PbX<sub>2</sub>/AA ink. After the liquid removal, the pellet was redispersed in DFP (50 mg mL<sup>-1</sup>).

**FET Fabrication:** For field-effect transistors, silicon with 200 nm of thermally grown SiO<sub>2</sub> was used as substrate material. The source and drain interdigitated electrodes were patterned by UV photolithography followed by e-beam evaporation of titanium and gold (5/40 nm). After the lift-off of excess photoresist and metal, the substrates were cleaned by sonicating them in acetone and isopropanol. Prior to active material deposition, the substrates were annealed for 5 min at 130 °C to remove remnants of solvents and moved to a nitrogen-filled glove box for further processing. The quantum dot film was deposited by means of blade-coating at 70 °C. Finally, samples were immersed in a methanol bath for 3 min to remove excess ligand species, then annealed for 30 min at 120 °C in case of PbS–PbX<sub>2</sub> QDs, and at 100 °C for PbS–MAPbI<sub>3</sub>.

The measured transistors with halide ligands have superior electron mobility ( $2.6 \times 10^{-3}$  vs  $4 \times 10^{-4}$  cm<sup>2</sup>V<sup>-1</sup>s<sup>-1</sup>) and on-off ratio ( $1.88 \times 10^6$  vs  $5.15 \times 10^4$ ) compared to their PbS–MAPbI<sub>3</sub> counterparts. Moreover, we observed a significant shift in threshold voltage from 6.02 V for PbS–PbX<sub>2</sub>/AA to 36.45 V for PbS–MAPbI<sub>3</sub> QDs.

**Current–Voltage Characterization and Neuromorphic Measurements:** The electrical characterization and neuromorphic measurements were performed using Keysight B2912A source-measurement unit with in-house-made Python software for FET, PPF, and STDP measurements and Keysight B2900 Quick IV Measurement Software for EPSC tracking. The data were acquired from samples kept under dark conditions in a nitrogen-filled glovebox.

### Supporting Information

Supporting Information is available from the Wiley Online Library or from the author.

### Acknowledgements

The authors would like to acknowledge the financial support of CogniGron - Groningen Cognitive Systems and Materials Center. The work was also supported by the European Union (ERC-AdvancedGrant, DEOM, 101055097). Views and opinions expressed are however those of the authors only and do not necessarily reflect those of the European Union or the European Research Council. Neither the European Union nor the granting authority can be held responsible for them. The authors thank A. Kamp and T. Zaharia for technical support, J. Pinna, L. Chen, and L. di Mario for discussions, and W. Talsma for the neuromorphic characterization software.

### Conflict of Interest

The authors declare no conflict of interest.

### Data Availability Statement

The data that support the findings of this study are available from the corresponding author upon reasonable request.

## Keywords

colloidal quantum dots, field-effect transistors, lead sulfide, ligand exchange, neuromorphic engineering, synaptic transistors

Received: April 28, 2023

Revised: July 13, 2023

Published online: August 27, 2023

- [1] J. Malmodin, D. Lundén, *Sustainability* **2018**, *10*, 3027.
- [2] F. Montecchi, T. Stickler, R. Hintemann, S. Hinterholzer, *Energy-Efficient Cloud Computing Technologies and Policies for an Eco-Friendly Cloud Market. Final Study Report*, European Commission, Vienna **2020**.
- [3] A. Mehonic, A. J. Kenyon, *Nature* **2022**, *604*, 255.
- [4] L. Chua, *Semicond. Sci. Technol.* **2014**, *29*, 104001.
- [5] E. Chicca, G. Indiveri, *Appl. Phys. Lett.* **2020**, *116*, 120501.
- [6] T. Qu, Y. Sun, M. Chen, Z. Liu, Q. Zhu, B. Wang, T. Zhao, C. Liu, J. Tan, S. Qiu, Q. Li, Z. Han, W. Wang, H. Cheng, D. Sun, *Adv. Mater.* **2020**, *32*, 1907288.
- [7] J.-Y. Chen, Y.-C. Chiu, Y.-T. Li, C.-C. Chueh, W.-C. Chen, *Adv. Mater.* **2017**, *29*, 1702217.
- [8] W. Li, P. Zhang, H. Li, X. Sheng, Y. Li, X. Xu, M. Yi, N. Shi, W. Shi, L. Xie, W. Huang, *Org. Electron.* **2019**, *75*, 105111.
- [9] L. Yin, C. Han, Q. Zhang, Z. Ni, S. Zhao, K. Wang, D. Li, M. Xu, H. Wu, X. Pi, D. Yang, *Nano Energy* **2019**, *63*, 103859.
- [10] M. Li, Z. Xiong, S. Shao, L. Shao, S. T. Han, H. Wang, J. Zhao, *Carbon* **2021**, *176*, 592.
- [11] L. Yin, W. Huang, R. Xiao, W. Peng, Y. Zhu, Y. Zhang, X. Pi, D. Yang, *Nano Lett.* **2020**, *20*, 3378.
- [12] W. Talsma, H. van Loo, S. Shao, S. Jung, S. Allard, U. Scherf, M. A. Loi, *Adv. Intell. Syst.* **2020**, *2*, 2000154.
- [13] M. Rinkio, A. Johansson, G. S. Paraoanu, P. Törmä, *Nano Lett.* **2009**, *9*, 643.
- [14] S. E. Cavanagh, L. T. Hunt, S. W. Kennerley, *Front. Neural Circuits* **2020**, *14*, 81.
- [15] M. Golesorkhi, J. Gomez-Pilar, F. Zilio, N. Berberian, A. Wolff, M. C. E. Yagoub, G. Northoff, *Commun. Biol.* **2021**, *4*, 970.
- [16] U. Hasson, J. Chen, C. J. Honey, *Trends Cognit. Sci.* **2015**, *19*, 304.
- [17] L. F. Abbott, W. G. Regehr, *Nature* **2004**, *431*, 796.
- [18] M. K. Kim, J. S. Lee, *Adv. Mater.* **2020**, *32*, 1907826.
- [19] R. A. John, N. Yantara, Y. F. Ng, G. Narasimman, E. Mosconi, D. Meggiolaro, M. R. Kulkarni, P. K. Gopalakrishnan, C. A. Nguyen, F. De Angelis, S. G. Mhaisalkar, A. Basu, N. Mathews, *Adv. Mater.* **2018**, *30*, 1805454.
- [20] S. Il Kim, Y. Lee, M. H. Park, G. T. Go, Y. H. Kim, W. Xu, H. D. Lee, H. Kim, D. G. Seo, W. Lee, T. W. Lee, *Adv. Electron. Mater.* **2019**, *5*, 1900008.
- [21] B. Jeong, P. Gkoupidenis, K. Asadi, B. Jeong, P. Gkoupidenis, K. Asadi, *Adv. Mater.* **2021**, *33*, 2104034.
- [22] M. Halter, L. Bégon-Lours, M. Sousa, Y. Popoff, U. Drechsler, V. Bragaglia, B. J. Offrein, *Commun. Mater.* **2023**, *4*, 14.
- [23] N. Sukharevska, D. Bederak, V. M. Goossens, J. Momand, H. Duim, D. N. Dirin, M. V. Kovalenko, B. J. Kooi, M. A. Loi, *ACS Appl. Mater. Interfaces* **2021**, *13*, 5195.
- [24] D. Bederak, D. M. Balazs, N. V. Sukharevska, A. G. Shulga, M. Abdu-Aguye, D. N. Dirin, M. V. Kovalenko, M. A. Loi, *ACS Appl. Nano Mater.* **2018**, *1*, 6882.
- [25] C. Ding, F. Liu, Y. Zhang, S. Hayase, T. Masuda, R. Wang, Y. Zhou, Y. Yao, Z. Zou, Q. Shen, *ACS Energy Lett.* **2020**, *5*, 3224.
- [26] X. Lan, O. Voznyy, A. Kiani, F. P. García De Arquer, A. S. Abbas, G. H. Kim, M. Liu, Z. Yang, G. Walters, J. Xu, M. Yuan, Z. Ning, F. Fan, P. Kanjanaboos, I. Kramer, D. Zhitomirsky, P. Lee, A. Perelgut, S. Hoogland, E. H. Sargent, *Adv. Mater.* **2016**, *28*, 299.
- [27] Y. Wang, K. Lu, L. Han, Z. Liu, G. Shi, H. Fang, S. Chen, T. Wu, F. Yang, M. Gu, S. Zhou, X. Ling, X. Tang, J. Zheng, M. A. Loi, W. Ma, *Adv. Mater.* **2018**, *30*, 1704871.
- [28] V. M. Goossens, N. V. Sukharevska, D. N. Dirin, M. V. Kovalenko, M. A. Loi, *Cell Rep. Phys. Sci.* **2021**, *2*, 100655.
- [29] A. G. Shulga, S. Kahmann, D. N. Dirin, A. Graf, J. Zaumseil, M. V. Kovalenko, M. A. Loi, *ACS Nano* **2018**, *12*, 12805.
- [30] D. M. Balazs, D. N. Dirin, H. H. Fang, L. Protesescu, G. H. Ten Brink, B. J. Kooi, M. V. Kovalenko, M. A. Loi, *ACS Nano* **2015**, *9*, 11951.
- [31] A. G. Shulga, L. Piveteau, S. Z. Bisri, M. V. Kovalenko, M. A. Loi, *Adv. Electron. Mater.* **2016**, *2*, 1500467.
- [32] D. Bederak, N. Sukharevska, S. Kahmann, M. Abdu-Aguye, H. Duim, D. N. Dirin, M. V. Kovalenko, G. Portale, M. A. Loi, *ACS Appl. Mater. Interfaces* **2020**, *12*, 52959.
- [33] D. Bederak, A. Shulga, S. Kahmann, W. Talsma, J. Pelanskis, D. N. Dirin, M. V. Kovalenko, M. A. Loi, *Adv. Electron. Mater.* **2022**, *8*, 2101126.
- [34] X. Yin, C. Zhang, Y. Guo, Y. Yang, Y. Xing, W. Que, *J. Mater. Chem. C* **2021**, *9*, 417.
- [35] R. Saran, R. J. Curry, *Nat. Photonics* **2016**, *10*, 81.
- [36] V. Sukhovatkin, S. Hinds, L. Brzozowski, E. H. Sargent, *Science* **2009**, *324*, 1542.
- [37] W. Zhou, Y. Shang, F. P. García de Arquer, K. Xu, R. Wang, S. Luo, X. Xiao, X. Zhou, R. Huang, E. H. Sargent, Z. Ning, *Nat. Electron.* **2020**, *3*, 251.
- [38] F. P. García de Arquer, D. V. Talapin, V. I. Klimov, Y. Arakawa, M. Bayer, E. H. Sargent, *Science* **2021**, *373*, <https://doi.org/10.1126/science.aaz8541>.
- [39] J. Owen, L. Brus, *J. Am. Chem. Soc.* **2017**, *139*, 10939.
- [40] Y. Pu, F. Cai, D. Wang, J. X. Wang, J. F. Chen, *Ind. Eng. Chem. Res.* **2018**, *57*, 1790.
- [41] D. N. Dirin, S. Dreyfuss, M. I. Bodnarchuk, G. Nedelcu, P. Papagiorgis, G. Itkos, M. V. Kovalenko, *J. Am. Chem. Soc.* **2014**, *136*, 6550.
- [42] I. Moreels, K. Lambert, D. Smeets, D. De Muyenck, T. Nollet, J. C. Martins, F. Vanhaecke, A. Vantomme, C. Delerue, G. Allan, Z. Hens, D. De Muyenck, T. Nollet, J. C. Martins, F. Vanhaecke, A. Vantomme, C. Delerue, G. Allan, Z. Hens, *ACS Nano* **2009**, *3*, 3023.
- [43] L. Cademartiri, E. Montanari, G. Calestani, A. Migliori, A. Guagliardi, G. A. Ozin, *J. Am. Chem. Soc.* **2006**, *128*, 10337.
- [44] Y. Kim, F. Che, J. W. Jo, J. Choi, F. P. García de Arquer, O. Voznyy, B. Sun, J. Kim, M. J. Choi, R. Quintero-Bermudez, F. Fan, C. S. Tan, E. Bladt, G. Walters, A. H. Proppe, C. Zou, H. Yuan, S. Bals, J. Hofkens, M. B. J. Roeffaers, S. Hoogland, E. H. Sargent, *Adv. Mater.* **2019**, *31*, 1805580.
- [45] D. M. Kroupa, M. Vörös, N. P. Brawand, B. W. McNichols, E. M. Miller, J. Gu, A. J. Nozik, A. Sellinger, G. Galli, M. C. Beard, *Nat. Commun.* **8**, **2017**, 15257.
- [46] S. Yin, C. H. Y. Ho, S. Ding, X. Fu, L. Zhu, J. Gullett, C. Dong, F. So, *Chem. Mater.* **2022**, *34*, 5433.
- [47] X. Liu, T. Fu, J. Liu, Y. Wang, Y. Jia, C. Wang, X. Li, X. Zhang, Y. Liu, *ACS Appl. Mater. Interfaces* **2022**, *14*, 14274.
- [48] H. Kim, M. I. Nugraha, X. Guan, Z. Wang, M. K. Hota, X. Xu, T. Wu, D. Baran, T. D. Anthopoulos, H. N. Alshareef, *ACS Nano* **2021**, *15*, 5221.
- [49] S. Liu, C. Zhang, S. Li, Y. Xia, K. Wang, K. Xiong, H. Tang, L. Lian, X. Liu, M. Y. Li, M. Tan, L. Gao, G. Niu, H. Liu, H. Song, D. Zhang, J. Gao, X. Lan, K. Wang, X. W. Sun, Y. Yang, J. Tang, J. Zhang, *Adv. Funct. Mater.* **2021**, *31*, 2006864.
- [50] Z. Huang, J. T. Koubek, A. Sellinger, M. C. Beard, *ACS Appl. Nano Mater.* **2022**, *5*, 3183.



- [51] C. Kim, J. Y. Kim, K. Lee, S. Y. Jung, D. J. Yun, T. K. An, H. S. Lee, Y. J. Jeong, J. Lee, *J. Ind. Eng. Chem.* **2020**, *85*, 111.
- [52] Z. Chen, Y. Yu, L. Jin, Y. Li, Q. Li, T. Li, Y. Zhang, H. Dai, J. Yao, *Mater. Des.* **2020**, *188*, 108415.
- [53] M. Kim, S. Oh, S. Song, J. Kim, Y. H. Kim, *Appl. Sci.* **2021**, *11*, 5020.
- [54] J. Bera, A. Betal, A. Sharma, U. Shankar, A. K. Rath, S. Sahu, *ACS Appl. Nano Mater.* **2022**, *5*, 8502.
- [55] X. Yan, Y. Pei, H. Chen, J. Zhao, Z. Zhou, H. Wang, L. Zhang, J. Wang, X. Li, C. Qin, G. Wang, Z. Xiao, Q. Zhao, K. Wang, H. Li, D. Ren, Q. Liu, H. Zhou, J. Chen, P. Zhou, *Adv. Mater.* **2019**, *31*, 1805284.
- [56] H. Zhang, Y. Zhang, Y. Yu, X. Song, H. Zhang, M. Cao, Y. Che, H. Dai, J. Yang, J. Yao, *ACS Photonics* **2017**, *4*, 2220.
- [57] N. Cowan, *Prog. Brain Res.* **2008**, *169*, 323.
- [58] T. Ohno, T. Hasegawa, T. Tsuruoka, K. Terabe, J. K. Gimzewski, M. Aono, *Nat. Mater.* **2011**, *10*, 591.
- [59] S. Kahmann, M. A. Loi, *Appl. Phys. Rev.* **2020**, *7*, 041305.
- [60] M. I. Nugraha, E. Yarali, Y. Firdaus, Y. Lin, A. El-Labban, M. Gedda, E. Lidorikis, E. Yengel, H. Faber, T. D. Anthopoulos, *ACS Appl. Mater. Interfaces* **2020**, *12*, 31591.
- [61] J. L. M. Abboud, R. Notario, *Pure Appl. Chem.* **1999**, *71*, 645.
- [62] R. S. Zucker, W. G. Regehr, *Annu. Rev. Physiol.* **2002**, *64*, 355.
- [63] H. Han, H. Yu, H. Wei, J. Gong, W. Xu, *Small* **2019**, *15*, 1900695.
- [64] M. Yarema, O. Yarema, W. M. M. Lin, S. Volk, N. Yazdani, D. Bozyigit, V. Wood, *Chem. Mater.* **2017**, *29*, 796.
- [65] L. H. Lai, L. Protesescu, M. V. Kovalenko, M. A. Loi, *Phys. Chem. Chem. Phys.* **2013**, *16*, 736.